Turbulence-Induced Anti-Stokes Flow and the Resulting Limitations of Large-Eddy Simulation

BRODIE PEARSON

Department of Earth, Environmental and Planetary Sciences, Brown University, Providence, Rhode Island

(Manuscript received 4 October 2017, in final form 16 November 2017)

ABSTRACT

This study shows that the presence of Stokes drift $\mathbf{u}_s$ in the turbulent upper ocean induces a near-surface Eulerian current that opposes the Stokes drift. This current is distinct from previously studied anti-Stokes currents because it does not rely on the presence of planetary rotation or mean lateral gradients. Instead, the anti-Stokes flow arises from an interaction between the Stokes drift and turbulence. The new anti-Stokes flow is antiparallel to $\mathbf{u}_s$ near the ocean surface, is parallel to $\mathbf{u}_s$ at depth, and integrates to zero over the depth of the boundary layer. The presence of Stokes drift in large-eddy simulations (LES) is shown to induce artificial energy production caused by a combination of the new anti-Stokes flow and LES numerics. As a result, care must be taken when designing and interpreting simulations of realistic wave forcing, particularly as rotation becomes weak and/or $\mathbf{u}_s$ becomes perpendicular to the surface wind stress. The mechanism of the artificial energy production is demonstrated for a generalized LES subgrid scheme.

1. Introduction

Surface gravity waves are ubiquitous within the global ocean. These waves induce a Lagrangian flow called the Stokes drift (Stokes 1847) that can affect the large-scale ocean currents as well as the small-scale mixing within the ocean surface boundary layer (OSBL). These two effects have largely been investigated separately, with the exception of some large numerical simulations (Hamlington et al. 2014; Suzuki et al. 2016).

The ocean currents are affected by surface waves in part because the Stokes drift imparts a Coriolis–Stokes force on the Eulerian flow, which must be balanced at large scales by an ''anti-Stokes'' Eulerian current or lateral pressure gradients. This type of anti-Stokes flow has been discussed in analytical (McWilliams and Restrepo 1999; Broström et al. 2008; McWilliams and Fox-Kemper 2013; Broström et al. 2014; Haney et al. 2015) and numerical modeling studies (Polton et al. 2005; Hamlington et al. 2014; McWilliams et al. 2014). Several studies have also discussed Eulerian flows induced by surface waves without planetary rotation. Monismith et al. (2007) found that a range of wave tank experiments exhibited Lagrangian (Stokes plus Eulerian) transport that was zero at all depths, possibly because of the experimental setup (Monismith et al. 2007; Weber 2011; Stuhlmeier 2015). Wave-induced Eulerian flows that balance the depth-integrated Stokes transport, leading to zero depth-integrated Lagrangian transport, have also been demonstrated in laminar fluids using nondispersive wave theory (Longuet-Higgins and Stewart 1962; McIntyre 1981; Groeneweg and Klopman 1998; van den Bremer and Taylor 2016). In contrast to the above work, we shall demonstrate an anti-Stokes current that has no depth-integrated Eulerian transport. In the tropical ocean, Smith (2006) observed a wave-induced Eulerian surface current, which balanced the surface Stokes drift of passing wave groups. The rapid distortion calculations of Teixeira (2011, 2012) suggest a partitioning of the turbulent shear stress that is consistent with the presence of Stokes drift and an opposingly sheared Eulerian current near the surface when the stress is zero.

Mixing in the OSBL is also affected by surface waves because Stokes drift can interact with OSBL turbulence to produce Langmuir turbulence, which is distinct from shear-driven turbulence and convection. In the past two decades large-eddy simulations (LES) of Langmuir turbulence have become possible (Skyllingstad and Denbo 1995; McWilliams et al. 1997). As a result of these LES, parameterizations for the properties of Langmuir turbulence have been developed (e.g., Harcourt and D'Asaro 2008;

Corresponding author: Brodie Pearson, brodie_pearson@brown.edu

DOI: 10.1175/JPO-D-17-0208.1

Grant and Belcher 2009), and the important role of Langmuir turbulence in the boundary layer and wider climate system has been diagnosed (Belcher et al. 2012; Li et al. 2016). With advancing time, studies have simulated Langmuir turbulence in ever more realistic and complex situations (McWilliams et al. 2012; Van Roekel et al. 2012; Kukulka et al. 2013; Pearson et al. 2015). Of particular relevance to the current paper is the trend toward simulations with nonparallel wind stress and Stokes drift vectors (e.g., Van Roekel et al. 2012; McWilliams et al. 2014; Rabe et al. 2015; Reichl et al. 2016).

In section 2, we demonstrate that the Stokes drift induces an anti-Stokes flow by interacting with OSBL turbulence. This anti-Stokes flow is antiparallel and comparable to the Stokes drift near the surface, is parallel to the Stokes drift at depth, integrates to zero over the depth of the OSBL, and does not require planetary rotation or alignment of wind and waves. In section 3, we demonstrate that the new anti-Stokes flow interacts with LES numerics to produce an artificial source of energy in LES of Langmuir turbulence, which could affect the properties of simulated turbulence. We summarize results in section 4.

2. Turbulence-induced anti-Stokes flow

The inviscid wave-averaged governing equations in the OSBL are given by (Craik and Leibovich 1976; McWilliams et al. 1997; Suzuki and Fox-Kemper 2016)

$$\frac{\partial \mathbf{u}}{\partial t} + \mathbf{u}\cdot\nabla\mathbf{u} + f\hat{\mathbf{z}}\times(\mathbf{u}+\mathbf{u}_s) = \mathbf{u}_s\times\omega - \nabla\left(p + \frac{1}{2}\mathbf{u}_s\cdot\mathbf{u}_s + \mathbf{u}_s\cdot\mathbf{u}\right) + b\hat{\mathbf{z}}, \tag{1}$$

where $\mathbf{u} = (u, v, w)$ is the Eulerian velocity, $\omega = \nabla\times\mathbf{u}$ is the vorticity, f is the Coriolis parameter, $\mathbf{u}_s = (u_s, v_s, 0)$ is the Stokes drift, p is the (density scaled) pressure, b is the buoyancy, and $\hat{\mathbf{z}}$ is the unit vertical vector. Equation (1) is often called the Craik–Leibovich equation. By taking a horizontal or temporal average of Eq. (1), we can separate the mean (overbar) and turbulent (prime) components of the velocity. For simplicity we shall consider horizontally homogeneous flows, in which all horizontal mean gradients are zero, then the y component of mean velocity evolves as

$$\frac{\partial \overline{v}}{\partial t} = -f(\overline{u} + u_s) - \frac{\partial \overline{v'w'}}{\partial z}. \tag{2}$$

If we now consider a scenario where $f = 0$ and the wind stress (which sets the surface boundary condition on $\overline{\mathbf{u}'w'}$) is aligned with the x direction, then Eq. (2) becomes a balance between the turbulent (Reynolds) stress gradient and the acceleration of the mean velocity:

$$\frac{\partial \overline{v}}{\partial t} = -\frac{\partial \overline{v'w'}}{\partial z}. \tag{3}$$

Equation (3) has two important implications in this scenario. First, if the depth profile of $\overline{v}$ reaches a steady state, the surface boundary condition (zero y stress) requires $\overline{v'w'} = 0$ at all depths. Second, integrating Eq. (3) over the boundary layer and using the zero-flux boundary conditions shows that the depth-averaged y velocity does not vary in time, as there is no injection of y momentum into the OSBL.

The above arguments are consistent with the no wave case ($\mathbf{u}_s = 0$, $f = 0$, wind stress in x direction), where $\overline{v}$ is constantly zero at all depths, but they also apply when there is a crosswind Stokes drift ($v_s \neq 0$, $u_s = 0$), where $\overline{v}$ becomes steady and depth varying (Fig. 1; this numerical simulation will be discussed in section 3). While the transition to the latter steady state must have $\overline{v'w'} \neq 0$ to redistribute y momentum vertically ($\partial\overline{v}/\partial t \neq 0$), here we shall focus on the final steady state of Eq. (3), where $\overline{v'w'} = 0$. We can understand why introducing a Stokes drift results in a nonzero $\overline{v}$ profile by looking at the budgets of the Reynolds stresses, found by multiplying the turbulent component of Eq. (1) by turbulent velocities and using the product rule

$$\frac{\partial \overline{u_i'u_j'}}{\partial t} = -\left(\overline{u_i'u_k'}\frac{\partial \overline{u_j}}{\partial x_k} + \overline{u_j'u_k'}\frac{\partial \overline{u_i}}{\partial x_k}\right) - \left(\overline{u_i'u_k'}\frac{\partial \overline{u_{sk}}}{\partial x_j} + \overline{u_j'u_k'}\frac{\partial \overline{u_{sk}}}{\partial x_i}\right) + D_{ij}, \tag{4}$$

where i, j, k can be 1, 2, or 3, indicating x, y and z components, respectively, and repeated indices are summed (subscript sk is the kth Stokes drift component). The left and right parenthetical quantities are the shear and Stokes terms, respectively. The term D_{ij} contains the buoyancy, Coriolis, advection, dissipation, and high-order (pressure and transport) terms (e.g., Harcourt 2013). In our scenario, we are particularly interested in the $\overline{v'w'}$ budget:

$$\frac{\partial \overline{v'w'}}{\partial t} = -\overline{w'w'}\frac{\partial \overline{v}}{\partial z} - \overline{v'v'}\frac{\partial \overline{v}_s}{\partial z} - \left(\overline{w'\frac{\partial p'}{\partial y}} + \overline{v'\frac{\partial p'}{\partial z}}\right) - \frac{\partial \overline{v'w'w'}}{\partial z} - \overline{v'b'} - f\overline{u'w'}, \tag{5}$$

where we have explicitly included the D_{23} terms. In the above steady state with Stokes drift, $\overline{v'w'}$ must constantly be zero, which means both sides of Eq. (5) must be zero.

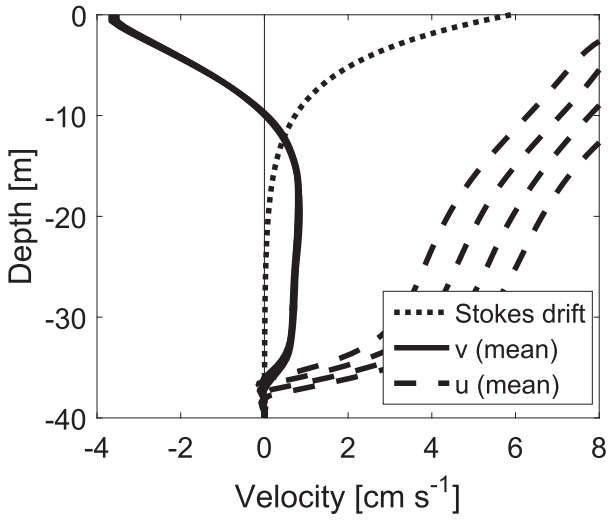

FIG. 1. Profiles of Eulerian and Lagrangian velocity components: $\overline{v}$ (solid), $\overline{u}$ (dashed), and v_s (dotted). The Eulerian currents are plotted for four consecutive averaging intervals; $\overline{u}$ accelerates, while $\overline{v}$ is steady with time.

In the OSBL velocity variances are positive and the Stokes drift distorts the turbulence (Teixeira and Belcher 2002) producing a Reynolds stress (in this case with $\partial v_s/\partial z > 0$ it produces negative $\overline{v'w'}$), which must be balanced by another term in Eq. (5). However, the transport term integrates to zero over the OSBL depth, the pressure terms cancel only a fraction of the production terms (Mironov 2009; Harcourt 2015), and in the current scenario the Coriolis term is zero and the buoyancy term is small. This means that the shear term in Eq. (5) must balance part of the Stokes term, which requires an Eulerian current with $\partial\overline{v}/\partial z < 0$ to develop near the surface that distorts the turbulence, producing positive $\overline{v'w'}$. An LES of the above scenario (described in section 3) does indeed have a leading-order balance in Eq. (5) between the Stokes and shear terms in the upper 20 m (not shown), with the pressure term being the next largest contributor.

The mean velocity required to balance the Stokes term near the surface has a vertical shear that opposes $\partial v_s/\partial z$. The velocity is also constrained to have zero mean when integrated over the boundary layer depth [Eq. (3)]. The LES results in Fig. 1 are consistent with this picture; there is a strong anti-Stokes (negative) current in the upper ocean, which changes rapidly with depth. This current becomes positive and weaker below the layer of significant Stokes shear, and the current shear is weak in the lower half of the mixed layer. There is current shear at the base of the mixed layer, which is not investigated here but could affect entrainment as the boundary layer grows into the thermocline.

The near-surface, anti-Stokes current is comparable, but not exactly equal, in magnitude to the Stokes drift but it arises from the Reynolds stress budgets, which makes prediction of this anti-Stokes current profile challenging. Analytic solutions for the current profile would require knowledge of the turbulence kinetic energy (TKE; $\overline{\mathbf{u}'\cdot\mathbf{u}'}/2$) and its anisotropy (e.g., $\overline{w'w'}/\overline{v'v'}$) as well as a deeper understanding of the high-order terms within Eq. (4). Developing a parameterization for the anti-Stokes flow profile from LES is also challenging for the reasons described in the next section.

In this section, we have demonstrated that an Eulerian anti-Stokes current arises from the wave-averaged (Craik–Leibovich) equations in the presence of turbulence. We considered a scenario where wind and waves are perpendicular and there is no planetary rotation, which isolated the anti-Stokes current, but the physical mechanism that drives the anti-Stokes current is present in any turbulent flow regardless of Coriolis parameter and the geometry of wind (or more generally surface stress) and wave forcing. For example, if the Stokes drift is not perpendicular to the surface stress ($u_s \neq 0$) then v_s (u_s) still induces a cross-wind (along wind) anti-Stokes current [Eq. (4) with $i, j = 2, 3$ (1, 3)], but the interaction between aligned wind and waves (Langmuir turbulence) would also affect the mean current, TKE anisotropy, and high-order terms in Eq. (4). Mechanisms for Reynolds stress production that are consistent with the possibility of an anti-Stokes Eulerian flow near the surface when wind and waves are aligned, and the surface stress is small, were discussed in Teixeira (2011). Alternatively, if we consider a rotating flow ($f \neq 0$), the total time-averaged, cross-wind, anti-Stokes current would become $\overline{v} = v_{ti} + v_{sc}$, where v_{ti} is the turbulence-induced flow discussed in this section. The other velocity component v_{sc} arises because the Stokes–Coriolis forces in Eq. (2) induce $\partial\overline{v'w'}/\partial z \neq 0$ and a resultant current that satisfies $\int v_{sc}\,dz = -\int v_s\,dz$ when integrated over the boundary layer (Broström et al. 2008; McWilliams and Fox-Kemper 2013) with $\partial v_{sc}/\partial z \neq 0$ analogous to the Stokes-modified Ekman spiral (Polton et al. 2005). The turbulence-induced anti-Stokes current, with $\int v_{ti}\,dz = 0$, would be required to ensure $\partial\overline{v}/\partial z$ maintains a steady crosswind momentum flux in Eq. (5); however, it is not clear at present how v_{sc} and v_{ti} could be uniquely diagnosed from the total current.

3. Resultant numerical effects in LES

The anti-Stokes current demonstrated in the previous section causes unphysical effects within large-eddy simulations. The equations of motion in LES are

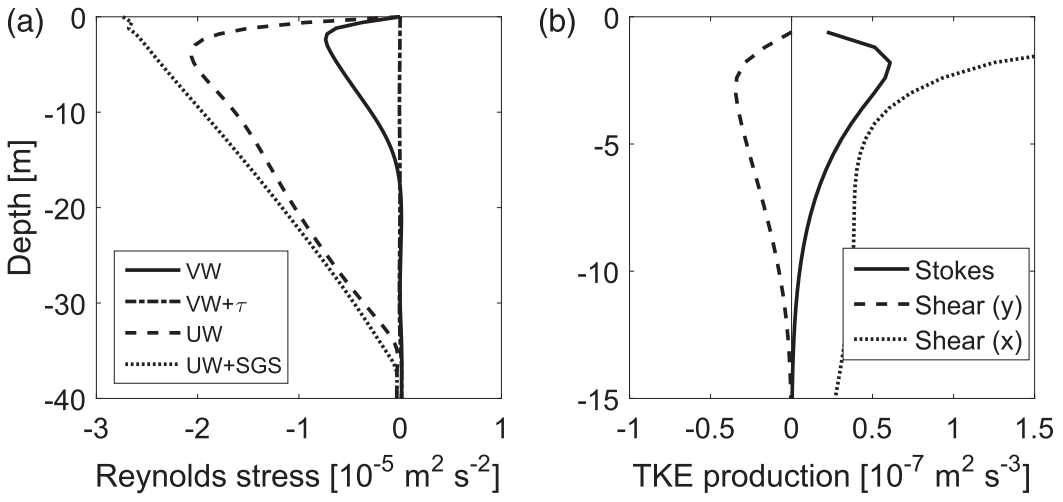

FIG. 2. Numerical effects of Eulerian anti-Stokes flow in LES. (a) Resolved Reynolds stresses, $\overline{v'w'}$ (solid) and $\overline{u'w'}$ (dashed), and total (resolved plus subgrid) stresses in the x (dotted) and y (dashed–dotted) directions. (b) Production of TKE by Stokes production ($-\overline{v'w'}\partial v_s/\partial z$; solid) and shear production in the y direction ($-\overline{v'w'}\partial\overline{v}/\partial z$; dashed) and x direction ($-\overline{u'w'}\partial\overline{u}/\partial z$; dotted). Note the different y-axis ranges.

similar to the above equations with the addition of a subgrid stress. In LES, Eq. (3) becomes

$$\frac{\partial \overline{v}}{\partial t} = -f(\overline{u} + u_s) - \frac{\partial \overline{v'w'}}{\partial z} - \frac{\partial \tau_y}{\partial z}, \tag{6}$$

where τ_y is the y component of subgrid stress. In this section, we will demonstrate that the anti-Stokes current induces a partitioning between the resolved Reynolds stress ($\overline{v'w'}$) and the subgrid stress τ_y. This leads to artificial (numerically induced) energy production.

The numerical effects are most easily seen if we consider the case from the previous section. We use the Met Office Large Eddy Model setup as described in Grant and Belcher (2009). Forcing consists of a constant x-aligned wind stress with friction velocity u_* and a constant Stokes drift [$v_s(z)$] aligned with the y axis and no rotation ($f = 0$). The Stokes drift is that of a monochromatic wave with $v_s(z) = v_{s0}\exp(z/\delta)$, where $v_{s0} = 5.9\,\mathrm{cm\,s^{-1}}$ and $\delta = 4.8\,\mathrm{m}$ with wind forcing $u_* = 0.09v_{s0}$. The resolution is $2(x)\,\mathrm{m} \times 2(y)\,\mathrm{m} \times 0.8(z)\,\mathrm{m}$, with $128 \times 128 \times 111$ grid points. The subgrid stress is modeled by a simple Smagorinsky scheme (Shutts and Gray 1994). Simulations are spun up from an at-rest 33-m-deep unstratified layer, with constant stratification below, for 60 000 s, and results are averaged over the next 40 000 s, except for the results shown in Fig. 1, which average over four separate 10 000-s intervals.

In the simulation there is no source of y momentum, and Fig. 1 shows that $\overline{v}$ is independent of time once the turbulence equilibrates. However, the LES integral condition on the stresses is now $\overline{v'w'} = -\tau_y$ at all depths, rather than the $\overline{v'w'} = 0$ condition of Eq. (3). One solution to this resolved and subgrid stress balance is that both terms are zero. However, this is not possible with extant LES because the anti-Stokes current has shear near the surface, leading to a subgrid stress under any LES scheme that follows the general form of $\tau_y = -\nu_t\partial\overline{v}/\partial z$, where ν_t is a positive, nonzero, parameterized LES subgrid viscosity (Smagorinsky 1963) that could depend on u_s (e.g., Sullivan et al. 2007). The presence of a subgrid stress requires that $\overline{v'w'}$ is equal and opposite in magnitude to τ_y, as seen in Fig. 2a. This is in contrast to the along-wind resolved momentum flux $\overline{u'w'}$, which has a much larger magnitude than its subgrid component within the interior of the OSBL.

The artificial momentum flux caused by the anti-Stokes current has an impact on the TKE production within the OSBL. Under the above forcing scenario outside LES, the anti-Stokes current is present, $\overline{v'w'} = 0$, and the budgets for each TKE component [Eq. (4) with $i = j$] have no production of $\overline{w'w'}$ by Stokes drift ($-2\overline{v'w'}\partial v_s/\partial z$) and no production of $\overline{v'v'}$ by current shear ($-2\overline{v'w'}\partial\overline{v}/\partial z$). In LES, by contrast, the artificial momentum flux always increases the Stokes production of $\overline{w'w'}$ and decreases the production of $\overline{v'v'}$ by the current shear. This implies partial compensation between artificial production in the total resolved TKE budget, as shown in Fig. 2b, in addition to compensation between these artificial resolved production terms and subgrid TKE production ($-\tau_y\partial v_s/\partial z$ and $-\tau_y\partial\overline{v}/\partial z$). However, it also shows that LES is not reliable for studying the properties of Langmuir turbulence when artificial Reynolds stresses are significant because TKE will be

unphysically partitioned across scales and directional velocity components. An example of this scenario, and the artificial Stokes production of TKE, can also be seen in Fig. 5e of Van Roekel et al. (2012), although it should be noted that their analyses use a large suite of rotating and nonrotating LES.

An artificial contribution to the along-Stokes Reynolds stress will be present in any LES with Stokes drift but will vary in importance across scenarios. For this reason we discourage LES in which the angle between wind and waves approaches 90° and as $f \to 0$, where the artificial effects become most important because the along-Stokes Reynolds stress, and the associated TKE production terms, would be minimal if there were no subgrid and artificial resolved stresses. Simulations of these scenarios could potentially be improved by modifying the subgrid scheme to include Stokes drift effects (e.g., Hamlington et al. 2014), although it is presently unclear how this should be approached. In other scenarios where the analytic along-Stokes–Reynolds stress and the associated TKE production terms are much greater than the artificial resolved stress and production terms, such as in Langmuir turbulence with aligned wind and waves, it is unlikely that artificial effects significantly change turbulent flow properties in LES.

4. Conclusions

We have shown that the Stokes drift interacts with turbulence in the ocean surface boundary layer to produce an Eulerian anti-Stokes current, which is distinct from other anti-Stokes currents related to the Stokes–Coriolis effect. Using the Craik–Leibovich wave-averaged equations we showed that the current is produced by the following mechanism:

1) In the presence of turbulence the Stokes drift produces a turbulent vertical flux of horizontal momentum (Reynolds stress).
2) A mean current with shear develops to produce an opposing Reynolds stress in order to maintain steady turbulence statistics.

Under constant forcing this anti-Stokes current reaches a steady state and has zero net Eulerian mass transport over the depth of the OSBL. The anti-Stokes flow partially cancels the Stokes drift mass transport near the surface and increases mass transport in the direction of Stokes drift deeper in the OSBL. As a result, the anti-Stokes flow could have implications for the lateral transport of tracers with depth-varying distributions.

In large-eddy simulations the anti-Stokes current causes artificial production of turbulence kinetic energy (TKE) through the following mechanism (continuing on from the above list):

3) Shear in the anti-Stokes current induces a LES subgrid stress.
4) The LES subgrid stress induces an equal and opposite "artificial" resolved Reynolds stress to satisfy integral constraints on momentum.
5) The artificial Reynolds stress changes the resolved production of TKE by Stokes drift and current shear.

A nonrotating simulation using perpendicular wind stress and Stokes drift demonstrated that the above process can induce Stokes production of vertical TKE and shear destruction of along-Stokes TKE, when the analytical solutions should have neither of these TKE budget terms. These results discourage performing LES in which the angle between wind and waves approaches 90° and as $f \to 0$ with present subgrid schemes.

Acknowledgments. I thank Alan Grant for many interesting discussions and two anonymous reviewers whose comments improved the presentation of these results. This work was supported by the National Environment Research Council under the OSMOSIS project NE/I020083/1, the National Science Foundation OCE 1350795, and the Office of Naval Research N00014-17-1-2963.

REFERENCES

Belcher, S. E., and Coauthors, 2012: A global perspective on Langmuir turbulence in the ocean surface boundary layer. *Geophys. Res. Lett.*, **39**, L18605, https://doi.org/10.1029/2012GL052932.

Broström, G., K. H. Christensen, and J. E. H. Weber, 2008: A quasi-Eulerian, quasi-Lagrangian view of surface-wave-induced flow in the ocean. *J. Phys. Oceanogr.*, **38**, 1122–1130, https://doi.org/10.1175/2007JPO3702.1.

——, ——, M. Drivdal, and J. E. H. Weber, 2014: Note on Coriolis-Stokes force and energy. *Ocean Dyn.*, **64**, 1039–1045, https://doi.org/10.1007/s10236-014-0723-8.

Craik, A. D. D., and S. Leibovich, 1976: Rational model for Langmuir circulations. *J. Fluid Mech.*, **73**, 401–426, https://doi.org/10.1017/S0022112076001420.

Grant, A. L. M., and S. E. Belcher, 2009: Characteristics of Langmuir turbulence in the ocean mixed layer. *J. Phys. Oceanogr.*, **39**, 1871–1887, https://doi.org/10.1175/2009JPO4119.1.

Groeneweg, J., and G. Klopman, 1998: Changes of the mean velocity profiles in the combined wave–current motion described in a GLM formulation. *J. Fluid Mech.*, **370**, 271–296, https://doi.org/10.1017/S0022112098002018.

Hamlington, P. E., L. P. Van Roekel, B. Fox-Kemper, K. Julien, and G. P. Chini, 2014: Langmuir–submesoscale interactions: Descriptive analysis of multiscale frontal spindown simulations. *J. Phys. Oceanogr.*, **44**, 2249–2272, https://doi.org/10.1175/JPO-D-13-0139.1.

Haney, S., B. Fox-Kemper, K. Julien, and A. Webb, 2015: Symmetric and geostrophic instabilities in the wave-forced ocean

mixed layer. *J. Phys. Oceanogr.*, **45**, 3033–3056, https://doi.org/10.1175/JPO-D-15-0044.1.

Harcourt, R. R., 2013: A second-moment closure model of Langmuir turbulence. *J. Phys. Oceanogr.*, **43**, 673–697, https://doi.org/10.1175/JPO-D-12-0105.1.

——, 2015: An improved second-moment closure model of Langmuir turbulence. *J. Phys. Oceanogr.*, **45**, 84–103, https://doi.org/10.1175/JPO-D-14-0046.1.

——, and E. A. D'Asaro, 2008: Large-eddy simulation of Langmuir turbulence in pure wind seas. *J. Phys. Oceanogr.*, **38**, 1542–1562, https://doi.org/10.1175/2007JPO3842.1.

Kukulka, T., A. J. Plueddemann, and P. P. Sullivan, 2013: Inhibited upper ocean restratification in nonequilibrium swell conditions. *Geophys. Res. Lett.*, **40**, 3672–3676, https://doi.org/10.1002/grl.50708.

Li, Q., A. Webb, B. Fox-Kemper, A. Craig, G. Danabasoglu, W. G. Large, and M. Vertenstein, 2016: Langmuir mixing effects on global climate: WAVEWATCH III in CESM. *Ocean Modell.*, **103**, 145–160, https://doi.org/10.1016/j.ocemod.2015.07.020.

Longuet-Higgins, M. S., and R. Stewart, 1962: Radiation stress and mass transport in gravity waves, with application to surf beats. *J. Fluid Mech.*, **13**, 481–504, https://doi.org/10.1017/S0022112062000877.

McIntyre, M., 1981: On the wave momentum myth. *J. Fluid Mech.*, **106**, 331–347, https://doi.org/10.1017/S0022112081001626.

McWilliams, J. C., and J. M. Restrepo, 1999: The wave-driven ocean circulation. *J. Phys. Oceanogr.*, **29**, 2523–2540, https://doi.org/10.1175/1520-0485(1999)029<2523:TWDOC>2.0.CO;2.

——, and B. Fox-Kemper, 2013: Oceanic wave-balanced surface fronts and filaments. *J. Fluid Mech.*, **730**, 464–490, https://doi.org/10.1017/jfm.2013.348.

——, P. P. Sullivan, and C. H. Moeng, 1997: Langmuir turbulence in the ocean. *J. Fluid Mech.*, **334**, 1–30, https://doi.org/10.1017/S0022112096004375.

——, E. Huckle, J.-H. Liang, and P. P. Sullivan, 2012: The wavy Ekman layer: Langmuir circulations, breaking waves, and Reynolds stress. *J. Phys. Oceanogr.*, **42**, 1793–1816, https://doi.org/10.1175/JPO-D-12-07.1.

——, ——, ——, and ——, 2014: Langmuir turbulence in swell. *J. Phys. Oceanogr.*, **44**, 870–890, https://doi.org/10.1175/JPO-D-13-0122.1.

Mironov, D. V., 2009: Turbulence in the lower troposphere: Second-order closure and mass–flux modelling frameworks. *Interdisciplinary Aspects of Turbulence*, W. Hillebrandt and F. Kupka, Eds., Lecture Notes in Physics, Vol. 756, https://doi.org/10.1007/978-3-540-78961-1_5,20161–222.

Monismith, S., E. Cowen, H. Nepf, J. Magnaudet, and L. Thais, 2007: Laboratory observations of mean flows under surface gravity waves. *J. Fluid Mech.*, **573**, 131–147, https://doi.org/10.1017/S0022112006003594.

Pearson, B. C., A. L. M. Grant, J. A. Polton, and S. E. Belcher, 2015: Langmuir turbulence and surface heating in the ocean surface boundary layer. *J. Phys. Oceanogr.*, **45**, 2897–2911, https://doi.org/10.1175/JPO-D-15-0018.1.

Polton, J., D. Lewis, and S. E. Belcher, 2005: The role of wave-induced Coriolis–Stokes forcing on the wind-driven mixed layer. *J. Phys. Oceanogr.*, **35**, 444–457, https://doi.org/10.1175/JPO2701.1.

Rabe, T. J., T. Kukulka, I. Ginis, T. Hara, B. G. Reichl, E. A. D. Asaro, R. R. Harcourt, and P. P. Sullivan, 2015: Langmuir turbulence under Hurricane Gustav (2008). *J. Phys. Oceanogr.*, **45**, 657–677, https://doi.org/10.1175/JPO-D-14-0030.1.

Reichl, B. G., D. Wang, T. Hara, I. Ginis, and T. Kukulka, 2016: Langmuir turbulence parameterization in tropical cyclone conditions. *J. Phys. Oceanogr.*, **46**, 863–886, https://doi.org/10.1175/JPO-D-15-0106.1.

Shutts, G. J., and M. E. B. Gray, 1994: A numerical modelling study of the geostrophic adjustment process following deep convection. *Quart. J. Roy. Meteor. Soc.*, **120**, 1145–1178, https://doi.org/10.1002/qj.49712051903.

Skyllingstad, E., and D. Denbo, 1995: An ocean large-eddy simulation of Langmuir circulations and convection in the surface mixed layer. *J. Geophys. Res.*, **100**, 8501–8522, https://doi.org/10.1029/94JC03202.

Smagorinsky, J., 1963: General circulation experiments with the primitive equations: I. The basic experiment. *Mon. Wea. Rev.*, **91**, 99–164, https://doi.org/10.1175/1520-0493(1963)091<0099:GCEWTP>2.3.CO;2.

Smith, J. A., 2006: Observed variability of ocean wave Stokes drift, and the Eulerian response to passing groups. *J. Phys. Oceanogr.*, **36**, 1381–1402, https://doi.org/10.1175/JPO2910.1.

Stokes, G. G., 1847: On the theory of oscillatory waves. *Trans. Cambridge Philos. Soc.*, **8**, 441–473.

Stuhlmeier, R., 2015: Gerstner's water wave and mass transport. *J. Math. Fluid Mech.*, **17**, 761–767, https://doi.org/10.1007/s00021-015-0219-4.

Sullivan, P. P., J. C. McWilliams, and W. K. Melville, 2007: Surface gravity wave effects in the oceanic boundary layer: Large-eddy simulation with vortex force and stochastic breakers. *J. Fluid Mech.*, **593**, 405–452, https://doi.org/10.1017/S002211200700897X.

Suzuki, N., and B. Fox-Kemper, 2016: Understanding Stokes forces in the wave-averaged equations. *J. Geophys. Res. Oceans*, **121**, 3579–3596, https://doi.org/10.1002/2015JC011566.

——, ——, P. E. Hamlington, and L. P. Van Roekel, 2016: Surface waves affect frontogenesis. *J. Geophys. Res. Oceans*, **121**, 3597–3624, https://doi.org/10.1002/2015JC011563.

Teixeira, M. A. C., 2011: A linear model for the structure of turbulence beneath surface water waves. *Ocean Modell.*, **36**, 149–162, https://doi.org/10.1016/j.ocemod.2010.10.007.

——, 2012: The influence of Langmuir turbulence on the scaling for the dissipation rate in the oceanic boundary layer. *J. Geophys. Res.*, **117**, C05015, https://doi.org/10.1029/2011JC007235.

——, and S. E. Belcher, 2002: On the distortion of turbulence by a progressive surface wave. *J. Fluid Mech.*, **458**, 229–267, https://doi.org/10.1017/S0022112002007838.

van den Bremer, T. S., and P. H. Taylor, 2016: Lagrangian transport for two-dimensional deep-water surface gravity wave groups. *Proc. Roy. Soc. London*, **A472**, 20160159, https://doi.org/10.1098/rspa.2016.0159.

Van Roekel, L. P., B. Fox-Kemper, P. P. Sullivan, P. E. Hamlington, and S. R. Haney, 2012: The form and orientation of Langmuir cells for misaligned winds and waves. *J. Geophys. Res.*, **117**, CO5001, https://doi.org/10.1029/2011JC007516.

Weber, J. E. H., 2011: Do we observe Gerstner waves in wave tank experiments? *Wave Motion*, **48**, 301–309, https://doi.org/10.1016/j.wavemoti.2010.11.005.